Iranian Polymer Journal (2018) 27:171–181
https://doi.org/10.1007/s13726-018-0598-5

ORIGINAL RESEARCH

A semi-conducting polypyrrole/coffee grounds waste composite for rhodamine B dye adsorption

Víctor M. Ovando-Medina[1] · Nancy E. Dávila-Guzmán[2] · Nancy V. Pérez-Aguilar[3] · Hugo Martínez-Gutiérrez[4] · Iveth D. Antonio-Carmona[5] · Silvia Y. Martínez-Amador[5] · Andrés Dector[6]

Received: 21 August 2017 / Accepted: 20 December 2017 / Published online: 13 January 2018

Abstract

A composite based on coffee grounds waste (CGW) coated with the semi-conducting polypyrrole (PPy) was prepared by pyrrole polymerization using potassium persulfate as oxidant. The composite was characterized by FTIR spectroscopy, cyclic voltammetry, UV/vis spectroscopy, scanning electron microscopy (SEM) and TGA analysis. SEM analysis showed homogeneous coating of coffee fibers with spherical nanoparticles of PPy with diameters in the range of 200–300 nm. Aqueous adsorption experiments of rhodamine B dye (RhB) onto the as-prepared composite were performed. The effect of pH and initial dye concentration (C_0) on the adsorption behavior was studied. The results showed that this material was an efficient adsorbent of RhB dye at alkaline pH. The adsorption experiments were set at $C_0 = 200$ mg/L and initial pH values of 2.0, 3.25 and 9.0, the adsorption capacities were 7.22, 13.8, and 19.0 mg of dye/g of the composite, respectively. Nonetheless, when pH was maintained at 9.0 throughout adsorption time, the adsorption capacity increased to 32 mg of dye/g of the composite. When performing adsorption tests using pure CGW, dye adsorption was insignificant at any pH level. Adsorption isotherm for RhB at controlled pH of 9.0 was well described by the Redlich–Peterson model and by the typical Langmuir adsorption model with a theoretical maximum adsorption capacity (q_{max}) of 50.59 mg of dye/g of composite.

Keywords Adsorption · Coffee grounds waste · Composite · Polypyrrole · Rhodamine B dye

Introduction

Water pollution with hazardous compounds has drawn global attention in the last decades due to its toxicity, abundance, and persistence. This pollution is attributed to population growth and intensive domestic activities, expanding industrial and agricultural production [1]. According to the United Nations World Water Development Report of 2017, about 80% of global wastewater is discharged without any treatment. The inadequate infrastructure in developing countries and the absence of technical capacity and financial resources explain the inefficiency of wastewater management [2]. One of the most polluting industries of water is the textile; where near to 200,000 tons of dyes are annually lost to effluents during the dyeing and finishing processes, due to the inefficiency of the dyeing process [3]. Usually, the treatment of dye polluted effluent can be done by adsorption, coagulation/flocculation, oxidation/ozonation, reverse osmosis, membrane filtration, biological degradation, electrochemical processes and photodegradation [4]. However, adsorption process is one of the most adopted treatment for

✉ Víctor M. Ovando-Medina
ovandomedina@yahoo.com.mx

1 Ingeniería Química, Coordinación Académica Región Altiplano (COARA), Universidad Autónoma de San Luis Potosí, 78700 Matehuala, SLP, Mexico

2 Facultad de Ciencias Químicas, Universidad Autónoma de Nuevo León, Av. Universidad, Cd. Universitaria, 66451 San Nicolás De Los Garza, NL, Mexico

3 Departamento de Ingeniería Química, Facultad de Ciencias Químicas, Universidad Autónoma de Coahuila, 25280 Saltillo, Coah, Mexico

4 Instituto Politécnico Nacional (IPN), Luis Enrique Erro S/N, 07738 Mexico, Mexico

5 Departamento de Botánica, Universidad Autónoma Agraria Antonio Narro, Calzada Antonio Narro 1923, Buenavista, 25315 Saltillo, Coah, Mexico

6 CONACYT - Universidad Tecnológica de San Juan del Río Av. La Palma 125, Col. Vista Hermosa, 76800 San Juan Del Río, Qro, Mexico

the removal of dye from aqueous solution due to its simplicity, high efficiency, easy recovery, and adsorbent reusability [5]. Therefore, the development of new materials of high performance, low cost and easy preparation in the adsorption of dyes from aqueous solution is an actual challenge.

One dye widely used as colorant and as tracer fluorescent is the RhB (Fig. 1), which is actually considered as toxic (such as reproductive and neurotoxicity) and carcinogenic (subcutaneous tissue borne sarcoma) [6, 7]. There is a great amount of studies dealing with RhB dye removal by adsorption using different adsorbent materials. For example, Bardajee et al. [8], prepared a composite of silver hydrogel of poly(acrylic acid) and salep (biopolymer) and used to remove RhB dye from aqueous solutions, observing that adsorption increased with the amount of the adsorbent, extraction time, stirring rate and solution volume, and decreased by increasing the temperature and pH of solution. In other work, Hayeeye et al. [9] used a composite of gelatin/activated carbon as adsorbent of RhB dye, and observed a maximum adsorption capacity of 256.41 mg of dye/g of adsorbent from the Langmuir isotherm. Shen et al. [10], prepared mesoporous silica nanosheets by electrospinning and calcination, and applied it to the adsorption of RhB from aqueous solutions. They observed a maximum adsorption capacity of 381.7 mg/g of adsorbent according to the Langmuir isotherm.

On the other hand, coffee grounds waste has been used in the removal of some dyes. Baek et al. [11] prepared degreased coffee-beans for the adsorption of malachite green (MG) dye from aqueous solution. It was observed that adsorbed amount of MG increased with the degreased coffee beans dosage and with the initial MG concentration. The adsorption isotherms were represented by the Langmuir and Freundlich models, with a maximum adsorption capacity of 55.3 mg/g. Hirata et al. [12] produced a carbonaceous material from coffee grounds and was employed in the removal of methylene blue and gentian violet dyes from wastewater, observing that the equilibrium adsorption data were represented with the Freundlich model. From their experimental data, a capacity adsorption of 55 mg of dye/g of adsorbent was observed. Coffee grounds waste has also been modified to be used as adsorbent of dyes, for example, Safarik et al.

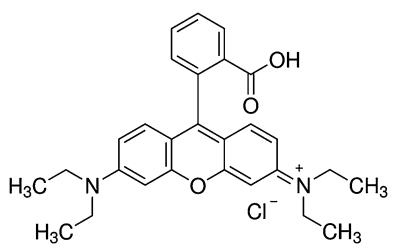

Fig. 1 Chemical structure of rhodamine B dye molecule

[13] modified coffee grounds waste mixing it with a ferrofluid to obtain a magnetic composite, which was used in the adsorption of different dyes included congo red dye (CR). They observed that adsorption data were well fitted by the Langmuir isotherm with a maximum capacity of 9.43 mg of CR dye/g of adsorbent. Shen et al. [7] used coffee waste powder in the removal of RhB, these authors observed a very low adsorption capacity of 5.25 μmol of dye/g of adsorbent (2.5 mg of dye/g of adsorbent).

It has been demonstrated that a combination of conducting polymers and cellulosic materials are good adsorbents of different compounds including some dyes [14]. Banimahd-Keivani et al. [15] used a composite of polyaniline/sawdust from walnut tree in the methylene blue removal from aqueous solutions. From their reported Langmuir isotherm data a maximum adsorption capacity of 8.3 mg/g was found. In another work, the same research team [16] used pyrrole instead of aniline and $FeCl_3$ as an oxidant to prepare the adsorbent composite and observed that maximum adsorption capacity was 34.3 mg/g. Following the Ansari et al. [15, 16] approach, we reported the polymerization of pyrrole onto sorghum waste fibers [17] to obtain a composite of sorghum/PPy which was used in the adsorption of methylene blue, and we observed that the adsorption mechanism was described by the Langmuir isotherm. In this respect the adsorption capacity of composite was 79.2 mg of dye/g of composite and the maximum adsorption capacity was 143.5 mg/g (66.4% more than the uncoated sorghum). In another work [18], our group reported the preparation of α-cellulose/PPy composite and succeeded to absorb reactive red dye. It was observed that for the adsorption experiments at an initial pH of 3.9, the adsorption capacity was 15.6 mg of dye/g of composite, whereas a value of 96.1 mg of dye/g of composite was obtained when the solution pH was set to 2.0. Adsorption isotherm was described by the typical Freundlich model. Also, a general three-resistance model that included the transport on the film that surrounds the composite particles, diffusion inside the particles, and adsorption on the surface of the particles was developed and achieved in transient adsorption process of RR120 on the synthesized composite.

Commercially available activated carbon and zeolites are often used in the removal of different pollutant from water, however they are very expensive. Therefore, the development of highly efficient materials, economic and of easy preparation is an important topic; particularly raw materials considered as wastes [19]. On this sense, the coffee industry produces large quantities of residues; among which, coffee grounds waste comprises the highest amount. Roughly 50% of the worldwide coffee production is processed for soluble coffee preparation, which generates until 6 million tons of CGW per year [20]. Therefore, the purpose of the present work was to prepare and characterize a low-cost composite

based on coffee grounds waste coated with a small amount of semi-conducting PPy. This composite was used in the removal of RhB dye from aqueous solutions.

Experimental

Materials

Pyrrole monomer, RhB, and potassium persulfate were purchased from Sigma-Aldrich (> 99%, Toluca, Mexico) and used as received. Coffee grounds waste (CGW) was obtained from a local cafeteria in Saltillo, Coah. (Mexico). Distilled and de-ionized water was used in all the experiments.

Methods

Synthesis of coffee grounds waste/polypyrrole composite

CGW at 100 g was washed twice with de-ionized water and dried at 60 °C through 48 h; this sample was labeled as M1. Afterwards, 50 g of the M1 sample was dispersed in 100 mL of a 0.1 N NaOH solution and decanted, and subsequently dispersed in 100 mL of a 0.1 N HCl solution. This sample was washed with de-ionized water until a pH of 6.5 was observed. Sample was dried at 60 °C through 48 h; this sample was labeled as M2. The semi-conducting CGW/PPy composite was prepared by mixing 15 g of CGW particles of M2 with 150 g of water, 4.5 g of ethanol, and 3.75 g of pyrrole into a beaker under magnetic stirring during 24 h. Afterwards, 7.55 g of potassium persulfate was added and allowed to react for 4 h. The resulting mixture (black dust) was filtered and washed with distilled water to eliminate unreacted components, and dried at 60 °C through 48 h; this sample was labeled as M3. The percentage of PPy coating α-cellulose fibers was determined by gravimetry giving a value of 6.7%.

Adsorption isotherms and kinetics determination

Adsorption experiments were carried out as follows: 125 mg of CGW/PPy composite was placed into 250 mL glass flasks containing 150 mL of RhB dye solution. The solutions were continuously stirred using an orbital shaker (150 rpm) at 25 °C until the equilibrium was achieved (120 min). The effect of pH on the adsorption capacity was evaluated at initial pH values of 2.0, 3.25 (natural pH of the RhB dye), and 9.0. An additional experiment was carried out at constant pH of 9.0 by additions of 0.1 N NaOH. Adsorption isotherms were performed at different RhB dye initial concentrations (100, 200, 400, 500, and 800 mg/L). Adsorption kinetics experiments were made at constant pH of 9 with 200 mg/L of initial RhB dye concentration, taking several samples at different times until an equilibrated concentration was reached. Concentrations of RhB dye solutions throughout adsorption experiments were determined in a spectrophotometer (Thermo, Genesis 10S UV/vis, USA) at $\lambda = 545$ nm using a calibration curve constructed with standard solutions. Adsorbed dye concentration at equilibrium (q) was calculated from a mass balance using the initial and final dye concentrations in the solutions.

Characterization

Point of zero charge (PZC) was determined as follows: in a conical vial the required volume of 0.1 M HCl or NaOH solution was mixed with the volume of a standard 0.1 N NaCl aqueous solution to achieve a final volume of 25 mL with pH in the range from 3.0 to 10.0 (pH_0). After 24 h under magnetic stirring, the pH of the resulting solutions was recorded (pH_{0f}). The same procedure of mixture preparation at different pH_0 was repeated but with the addition of 0.1 g of composite and, after 48 h of equilibration pH was measured (pH_f). Data of $\Delta pH = (pH_f – pH_{0f})$ as a function of pH_{0f} was calculated.

The uncoated CGW (M2 sample) and the CGW/PPy (M3 sample) composites were characterized by scanning electron microscopy (Jeol, JSM 7800F, Japan). The samples were also analyzed by FTIR (Agilent, Cary 630, USA). The electrochemical response of CGW/PPy was verified by cyclic voltammetry (CV) experiments dispersing 50 mg of the composite in 100 mL of 0.1 N potassium sulfate aqueous solutions at 150 mV/s of scan rate at room temperature (25 °C). Pt electrode was used as working electrode; Ag/AgCl saturated in KCl was used as reference electrode and a Pt wire as counter-electrode. Voltage and current measurements were monitored using a GAMRY (G300, USA) potentiostat/galvanostat. The UV/vis spectrum of CGW/PPy composite was recorded by dispersing 12 mg of composite in 3 mL of de-ionized water using an ultrasonic processor (Cole–Parmer™). The specific surface area (A_{BET}) of composite was determined by N_2 physisorption (Quantachrome Instruments, USA) using the Brunauer, Emmett, Teller (BET) method. Thermal stability of pure α-cellulose, magnetite, and composite was studied by thermogravimetric analysis (Setaram, Setsys Evolution, USA), for this 10 mg of each sample was heated between 25 and 800 °C at a heating rate of 10 °C/min.

Results and discussion

Composite characterization

Figure 2 shows the SEM images of CGW washed with water (Fig. 2a, b) and CGW after washing with 0.1 N NaOH and

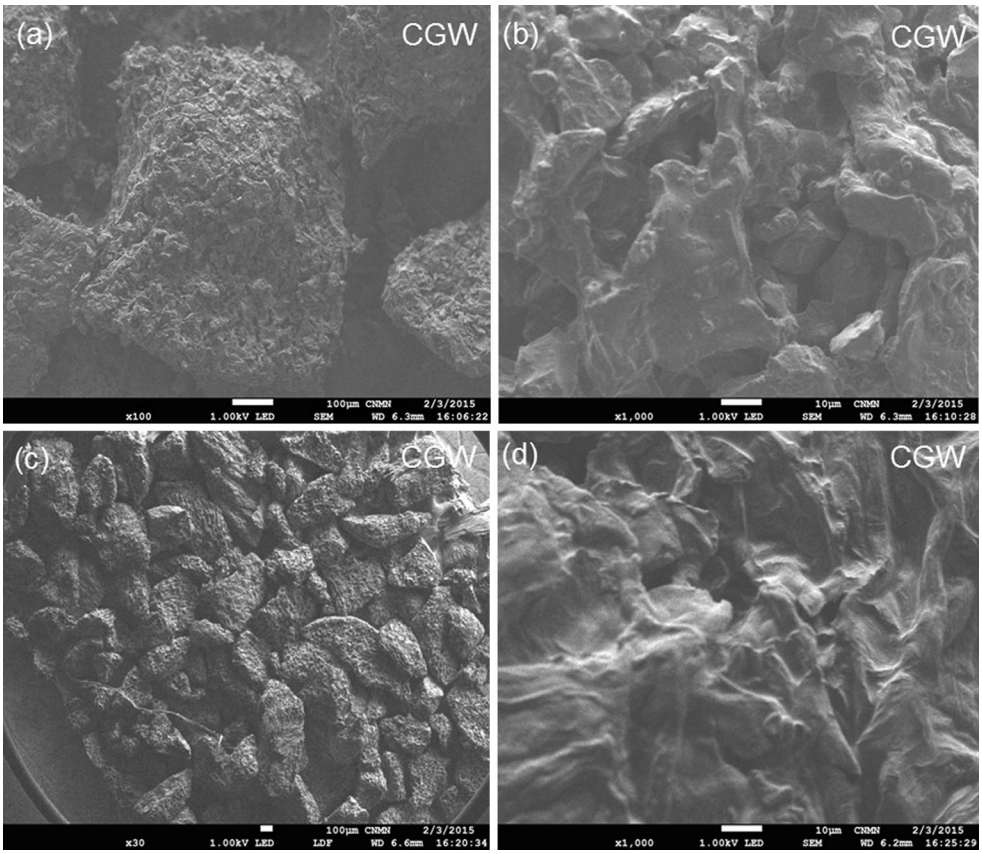

Fig. 2 SEM images of CGW washed with water (**a**, **b**) and with 0.1 N NaOH and HCl aqueous solutions (**c**, **d**)

HCl aqueous solutions (Fig. 2c, d) at two different magnifications. It can be seen that CGW consisted of porous grains with sizes in the range of 200–600 µm formed by fibers with flat surface. It is observed that after basic and acid treatments the surface remains unaffected, and only soluble compounds were extracted. Figure 3 shows the SEM images of CGW/PPy composite. Clearly, the pores were filled with agglomerated PPy nanoparticles of spherical morphology with sizes in the interval of 100–250 nm. The spherical shape of PPy particles has been reported for pyrrole aqueous solution polymerization; however, particles sizes depended on the surface on which they were growing. For example, when polymerized onto sorghum cellulosic fibers particles with average size of 120 nm were obtained [17]. However, by using $FeCl_3$ as an oxidizing agent in the pyrrole polymerization onto cellulose fiber, PPy nanoparticles of sizes between 50 and 150 nm [21] were produced.

The CGW contains large amounts of organic compounds as fatty acids, lignin, cellulose, hemicellulose, and other polysaccharides [22]. In this work, we analyzed M2 and M3 samples which were washed with water, NaOH and HCl solutions, respectively. Therefore, most soluble compounds were removed, and it was expected that cellulose would remain as the main component of the samples. Cellulose is arranged in micro-fibrils enclosed by hemicellulose and lignin [23]. The molecular structure of cellulose gives some advantages including low density, recyclability, and biodegradability [24]. Also due to the high donor reactivity of the hydroxyl group, which has a tendency to form intra- and inter-molecular hydrogen bonds, a broad chemical variability is expected. These characteristics make cellulose a potential material in making composites [18]. Figure 4 shows the FTIR spectra of uncoated CGW, PPy and CGW/PPy composite. It can be seen that the characteristic signals corresponding to cellulose of CGW [22] and PPy are present. It can also be observed that the spectrum for the CGW/PPy composite is similar to that corresponding to CGW, with the main difference at 1545 cm^{-1}; which is related to a mixed C=C and inter-ring C–C vibrations of PPy units. The peak at 1465 cm^{-1} derives from C–C PPy ring stretching as can be observed in the FTIR spectrum of PPy alone (inset in Fig. 4) [18]. It is also observed that cellulose of CGW signals corresponding to O–H and C–H stretching (3200 and 3400 cm^{-1}) are not present in the composite; and signals of C-H in aliphatic chains (2900 and 2853) are weaker in the composite, which can be ascribed to the presence of PPy coating CGW cellulose fibers. Chemical bonding between cellulose fibers of CGW and PPy is desirable because PPy would be more

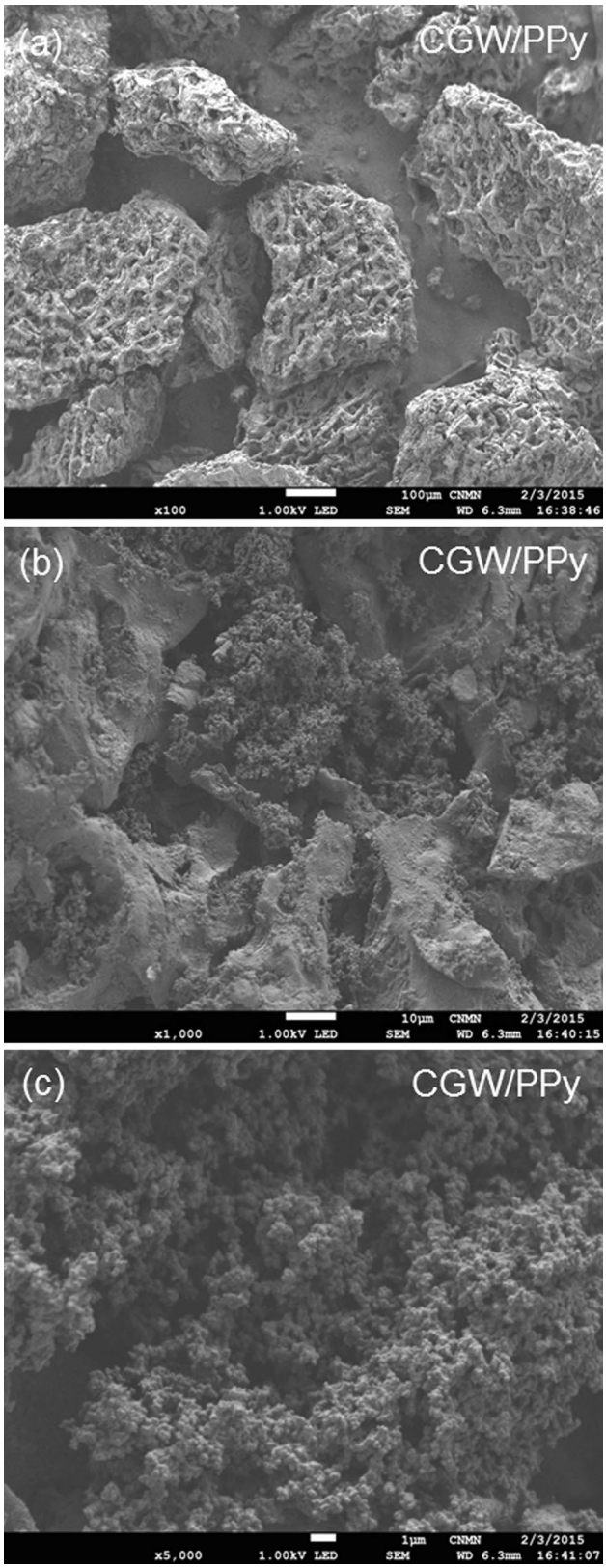

Fig. 3 SEM images of CGW/PPy composite at different magnifications

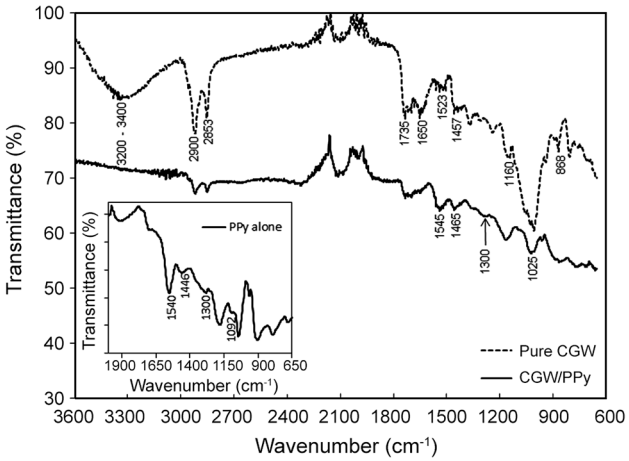

Fig. 4 FTIR spectra of CGW, PPy and CGW/PPy composite

difficult to separate from the cellulose of CGW. It would be expected that this bonding would form through –OH groups of cellulose and the –NH groups of PPy rings. From Fig. 4, it can be observed that bands at 1540 and 1446 cm^{-1} for PPy alone (inset in Fig. 4) are shifted to 1545 and 1465 cm^{-1} for the composite. The observed shift of these bands are due to chemical bonding between –NH in the pyrrole ring units and the –OH groups of cellulose [25, 26].

PPy presence onto CGW/PPy composite can also be demonstrated by UV/vis analysis. Figure 5 shows the UV/vis spectra of uncoated CGW, CWG/PPy composite and just PPy. Sample corresponding to CGW showed only an absorbance band between 250 and 400 nm of wavelength, which can be ascribed to cellulosic fibers and other compounds of coffee grounds waste like different chromophores that are formed from polysaccharides during the thermal-oxidative

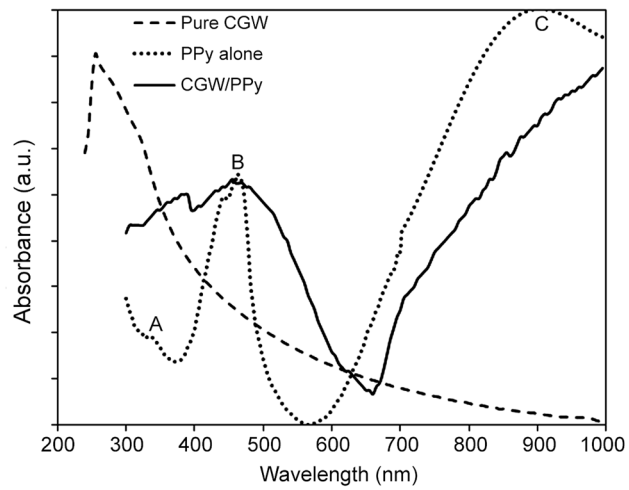

Fig. 5 UV/Vis spectra of uncoated CGW, PPy and CWG/PPy composite

stress in the roasting process [27]. On the other hand, CGW/PPy composite and PPy alone show three well-defined adsorption bands in the UV/vis spectrum of Fig. 5. The first band between 300 and 370 nm (labeled as A in Fig. 5) is usually ascribed to π–π^* transition of the pyrrole moiety. Absorption labeled as B in the UV/vis spectrum is assigned to the high-energy polaron transition along the PPy chains [28], and is indicative of α–α coupling of pyrrole radical-cations during PPy chain growth, and is related to chain planarity and linearity, the higher the chain linearity, the higher the PPy macroscopic conductivity [29]. The third absorption band centered at around 900 nm (labeled as C in Fig. 5) is due to PPy bipolaron state (the fully oxidized black form of PPy). Bipolaron state is observed when some dopant agent is present in the conducting polymer chain, in our case; the bipolaron state can be due to the presence of remaining coffee compounds acting as dopant agents by associating with the positive form of PPy [30]. Detailed information on chemical polymerization mechanism of pyrrole, chain structure and properties can be found in the literature [29].

Thermal stability is an important characterization because it determines the temperature at which the composite degradation is not present and adsorption process can be achieved. The thermograms (TGA) of CGW, PPy and CGW/PPy composite in the range of room temperature to 800 °C are shown in Fig. 6. CGW shows four well-defined weight loss stages. The first change is around 100 °C and corresponds to water evaporation. The second transformation occurs at approximately 307 °C; at this stage, the depolymerization and decomposition of polysaccharides [31], and some oils present in the sample occur, providing weight losses of 22%; a third change was observed at 347 °C when 42.6% of weight loss has been achieved. The last thermal stage related to the total decomposition of the samples starts at 600 °C for a weight loss of 76%. In the case of the composite, only two important transformations are observed, the first change was at lower temperature (292 °C) with 25% of weight loss, and the total degradation of composite at 600 °C with 65% of weight loss. The lower thermal stability of composite with respect to uncoated CGW is due to the presence of PPy which decomposes at lower temperature (150–250 °C) [32]. However, decomposition rate of CGW/PPy composite is slower than the corresponding uncoated CGW.

N_2 adsorption/desorption isotherms of CGW and CGW/PPy composite are shown in Fig. 7a. It can be seen that the uncoated CGW has higher porosity than CGW/PPy composite; however, the adsorbed N_2 amount is very low in both samples. The hysteresis phenomenon of nitrogen adsorption/desorption isotherms can be associated with the capillary condensation in mesoporous structures. Different forms of the hysteresis loop are caused by different types of adsorbent and sorption environments (as temperature and pressure) [33]. According to IUPAC, pores are classified in

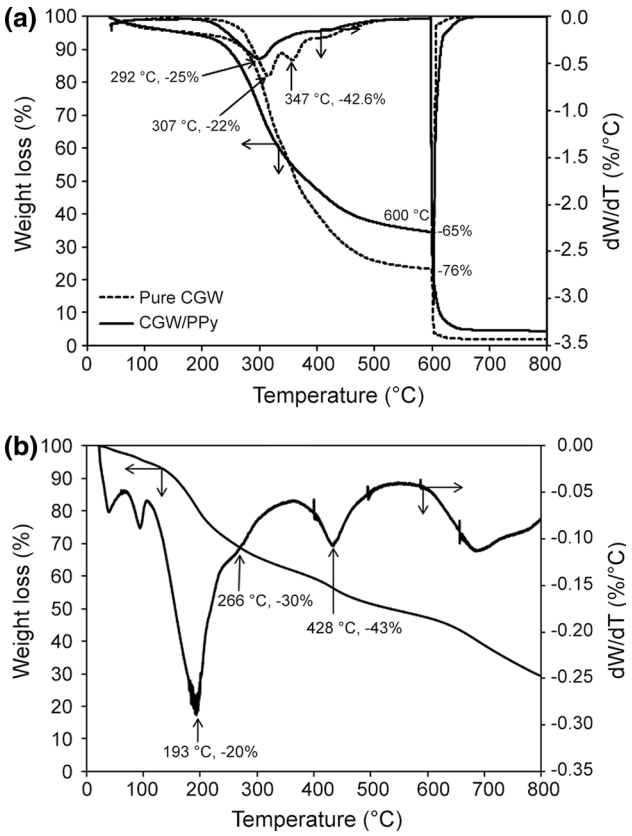

Fig. 6 TGA curves and its derivatives of CGW and CGW/PPy composite **a**, and PPy alone **b**

macropores (≥ 50 nm), mesopores (2–50 nm), and micropores (≤ 2 nm) [34], whereas hysteresis loops are classified in four types from H1 to H4 [35]. In our curves, shown in Fig. 7a, it corresponds to H3 hysteresis loop type and as observed by Ballesteros et al. [31] for CGW alone, no micropores were observed, because there is no tendency to form a plateau at relatively low pressures (stepped isotherm shape). The BET area (A_{BET}) of CGW/PPy composite is decreased by about 2.2 times compared to uncoated CGW, which can be ascribed to deposition of PPy nanoparticles coating CGW pores (Fig. 3a), and pores of resulting composite are mainly due to PPy interparticle spaces.

The electric properties such as surface charge of a solid in contact with an aqueous solution play an important role in interfacial and colloidal phenomena, as well as in adsorption. The experimental curves of PZC determination are presented in Fig. 7b. These results indicate that PZC values are 5.4 and 3.2 for CGW and CGW/PPy composite, respectively. Therefore, pH values during RhB dye adsorption experiments should be maintained above 3.2 in order to ensure a negatively charged composite surface. At lower pH values, the surface charge becomes positively charged, and H^+ ions compete effectively with the RhB cations and thus a

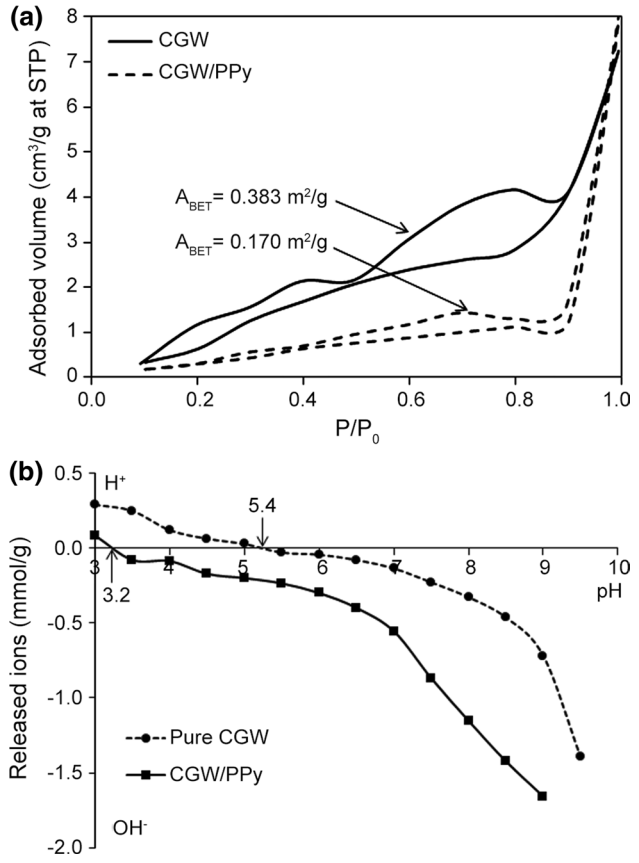

Fig. 7 N_2 adsorption/desorption isotherms **a**, and PZC **b** of CGW and CGW/PPy composite

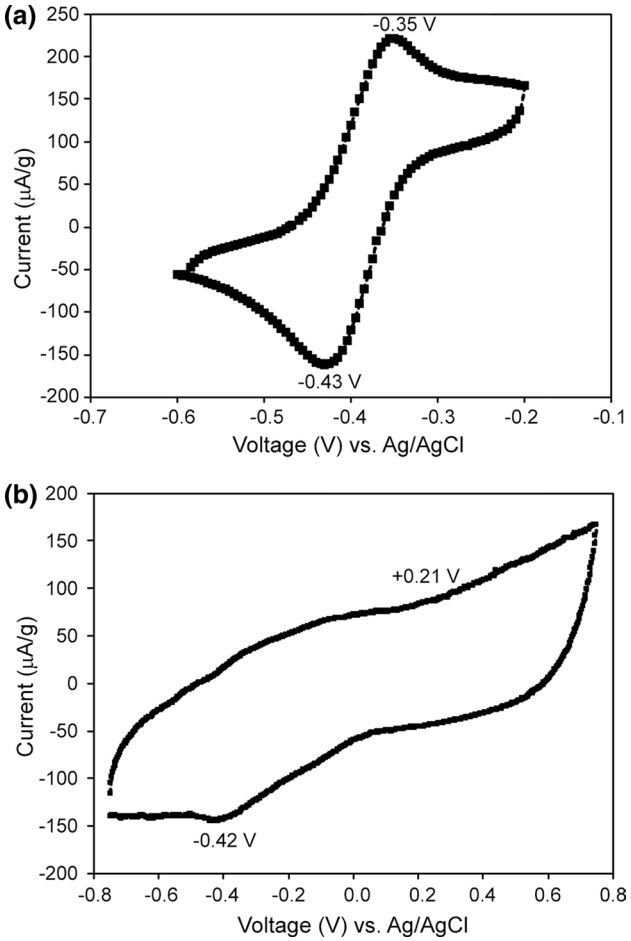

Fig. 8 Cyclic voltammetry of CGW/PPy composite **a** and alone PPy **b** at 150 mv/s of scan rate

decrease in the amount of dye adsorbed would be expected. Franca et al. [36] studied the adsorption of methylene blue dye (cationic) onto CGW and they found that ZPC of CGW was in the range of 3.4–3.6, the lower value with respect to our CGW (5.4) which can be due to the NaOH and HCl treatments before PZC determination.

The electrochemical performances of CGW/PPy and just PPy were carried out by cyclic voltammetry. The CV curve of CGW/PPy is displayed in Fig. 8a at a scan rate of 150 mV s^{-1} between − 0.6 and − 0.2 V vs. Ag/AgCl in 0.1 N K_2SO_4 as electrolyte. It can be seen that CV curve of CGW/PPy shows a characteristic oxidation and reduction behavior of the obtained polymer [37, 38]. During the positive potential scan this curve shows a broad anodic peak at a potential of − 0.35 V vs Ag/AgCl and in the negative scan a cathodic peak at − 0.43 V vs. Ag/AgCl. Finally, a current at the oxidation peak of 221 μA/g was achieved. Figure 8b shows the electrochemical response of PPy alone. A weak cathodic peak for PPy can be seen at approximately + 0.21 V. The CGW/PPy shows an increment in the current with respect to PPy (75 μA/g). Besides, a considerable shift of the anodic and cathodic potential peaks was observed; the anodic peak shifted from − 0.4 to − 0.43 V vs. Ag/AgCl, for PPy and CGW/PPy, respectively; whereas the cathodic peak shifted from + 0.21 to − 0.3 V vs. Ag/AgCl for PPy and CGW/PPy, respectively. Thus, the presence of CGW in the composite has a strong effect on electrochemical behavior of composite due to chemical interaction between PPy and the CGW. Comparing Fig. 2d with Fig. 3b, we can say that some of PPy spheres are in fact fused together to form an integral heterogeneous film and clusters on the CGW pores and surface. After ultrasonication of the composite we do not observe PPy removal, which can suggest chemical bonds exist between PPy and cellulose of CGW through –NH group of PPy and HO– from cellulose of CGW [25]. This chemical interaction would explain the shift of oxidation and reduction potentials observed by the CV experiments.

Rhodamine B adsorption

Effect of pH

Adsorption mechanisms of the RhB dye onto the CGW/PPy composite can be as followings: attachment through π–π*

(bonding/anti-bonding) interactions between the electrons of the aromatic rings of the dye molecules and the electrons of pyrrole rings. High affinity of the dye for the composite surface can also result from hydrogen bond formation, which can be created between nitrogen from the pyrrole ring and nitrogen of the $–NH_2$ group of the dye. Due to the conducting properties of PPy and charge transport, the effect of pH on the adsorption capacity was evaluated as shown in Fig. 9. The acidity of the RhB dye solutions had a negative effect on the CGW/PPy adsorption capacity, decreasing 2.64 folds when the initial pH was diminished from 9 to 2 (diamonds and squares, respectively on Fig. 9). Thus, the adsorption capacity was favored at basic pH conditions. According to the speciation diagram, at pH solutions lower than 4.0, the RhB dye exists in its cationic form [39], meanwhile the CGW/PPy surface is predominantly positive, since the PZC is 3.2, which causes repulsion between RhB dye molecules and the surface of the composite would decrease the adsorption capacity. At pH above 6, the RhB dye has positive and negative charges and the CGW/PPy has a surface with a net negative charge which may lead to favorable electrostatic interactions, increasing the adsorption capacity. Additionally, in the adsorption experiments it was observed

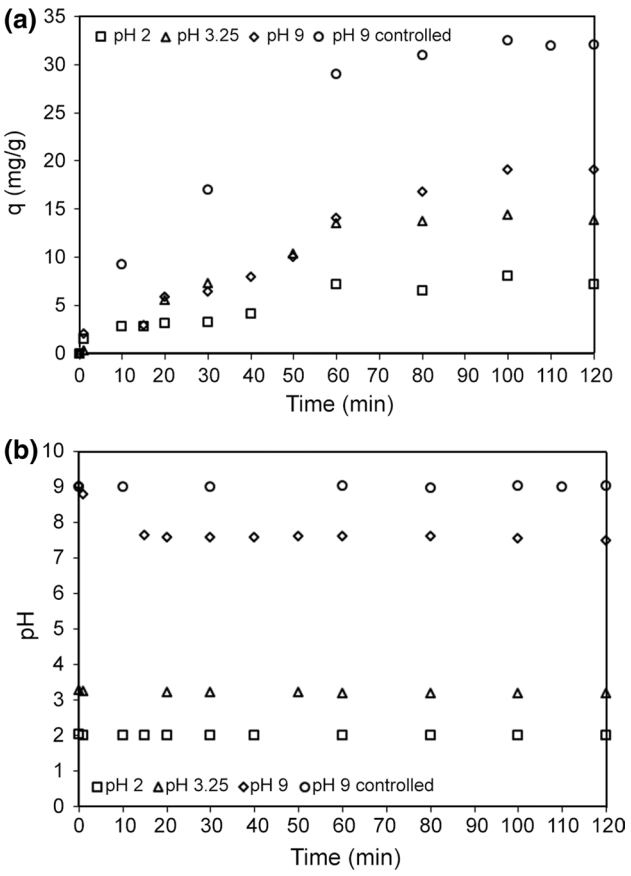

Fig. 9 **a** Kinetics of RhB dye uptake, q, and **b** change of the solution pH through adsorption experiments at initial concentration of 200 mg/L and different initial pH (CGW/PPy mass of 125 mg)

that the pH was constant when the initial pH was set to 2.0 and 3.25, while at initial pH of 9.0, the final pH registered decreased to 7.47 (Fig. 9b). Therefore, an additional experiment was performed controlling pH at a constant value of 9.0. The adsorption capacity under this condition increased by 4.4, 2.3, and 1.7 times compared to the experiments with initial pH of 2.0, 3.25 and 9.0 (uncontrolled), respectively. These results indicate that the pH solution has a significant role in the RhB adsorption capacity onto CGW/PPy.

Adsorption isotherm

Adsorbents behavior can be described by adsorption isotherms. Modeling the adsorption isotherms data is useful to compare different materials; because it permits the optimization of the adsorption processes, and to determine the maximum adsorption capacities, allowing good adsorption systems design [40]. In the present work, the adsorption isotherm was determined at room temperature (25 °C) and constant pH of 9, to evaluate the saturation of the CGW/PPy. As can be seen in Fig. 10a, the adsorption isotherm has reached a plateau, according to the classification of solution adsorption isotherms; this is a Type L (Langmuir) adsorption isotherm which would indicate a monolayer adsorption behavior [41].

The Langmuir model is a theoretical model that assumes adsorption forces strong enough to cover the surface of the adsorbent by a monomolecular layer of adsorbate of approximately one molecule in thickness in many cases [42]. Equation 1 represents the Langmuir model, where q_{max} is the theoretical maximum adsorption capacity in mg/gat very high dye equilibrium concentration, K_L is the Langmuir parameter in L/mg, C_e is the equilibrium concentration in mg/L and q is the equilibrium adsorption capacity in mg/g:

$$\text{Langmuir model}: q = \frac{q_{\max} K_L C_e}{1 + K_L C_e} \quad (1)$$

Furthermore, a dimensionless separation factor, R_L, has been defined for the Langmuir model to indicate the type of the adsorption to be either irreversible ($R_L = 0$), favorable ($0 < R_L < 1$), linear ($R_L = 1$), or unfavorable ($R_L > 1$) as follows:

$$R_L = \frac{1}{1 + K_L C_0} \quad (2)$$

where, C_0 is the initial RhB concentration in mg/L.

On the other hand, the Freundlich model is an empirical model that has been used to describe the adsorption equilibrium of adsorbents with energetically heterogeneous surfaces [43]:

$$q = K_F C_e^{1/n} \quad (3)$$

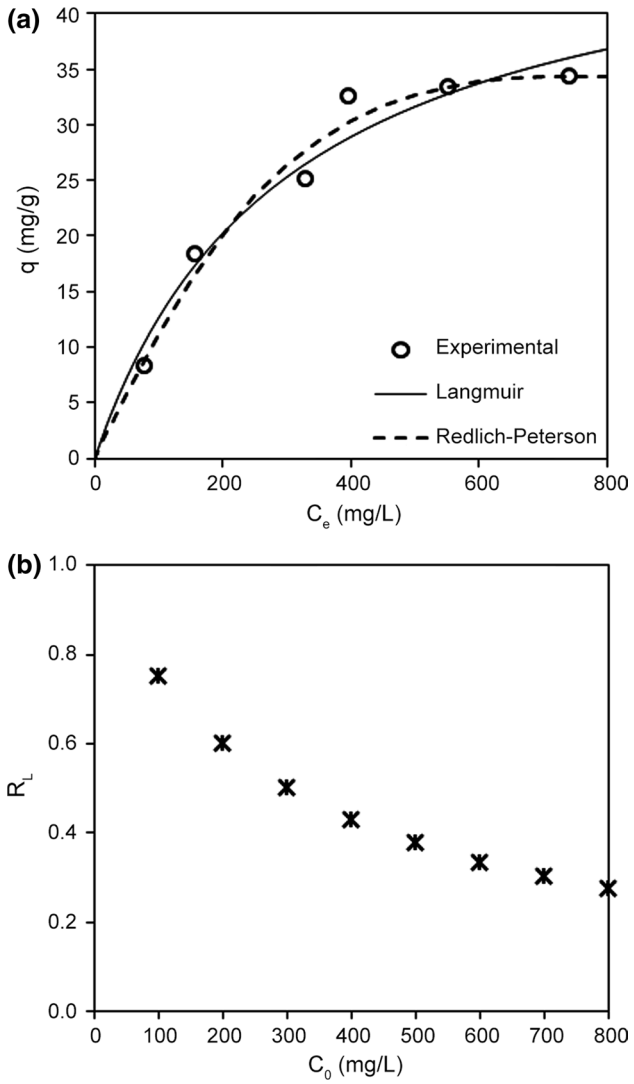

Fig. 10 **a** Adsorption isotherm of RhB at controlled pH of 9 and **b** separation factor (R_L) calculated at different initial RhB dye concentrations

where K_F (mg/g (L/mg)$^{1/n}$) and n (dimensionless) are the Freundlich parameters.

The other isotherm model is the Redlich–Peterson, which includes three adjustable parameters into an empirical isotherm. It has been useful to fit adsorption isotherm data behavior between Langmuir and Freundlich mechanisms (homogeneous and heterogeneous surface). This model is expressed as [44]:

$$q = \frac{K_{RP} C_e}{1 + a_R C_e^{\beta}} \tag{4}$$

where K_{RP}, a_R and β are the Redlich–Peterson parameters. If the value of β is 1, the equation is reduced to the Langmuir model, when the $a_R C_e^{\beta}$ is $\gg 1$, it reduces to Freundlich isotherm. The K_{RP}/a_R ratio indicates the adsorption capacity.

As can be seen in Table 1, not only the correlation coefficient (R^2) was higher for the Langmuir model compared to the Freundlich model, as we expected from the solution adsorption isotherms classification, but also lower deviation percentage (% D) was obtained for the Langmuir model. The parameters of the Langmuir isotherm, q_{max} and K_L, were 50.59 mg/g and 0.00333 L/mg, respectively; the former is associated to the maximum adsorption capacity while the latter is related to the affinity of the binding sites. Also, the R_L separation factor values were in the range of 0.75–0.27 (Fig. 10b), which indicates a favorable adsorption process of RhB dye.

The calculated parameters of Redlich–Peterson isotherm, and the % D and R^2 values are given in Table 1. Obviously, the higher the parameters number in a model, the higher the R^2 values; however, the lower %D observed for this model (6.0%) and the random distribution of residuals calculated from the difference between calculated and experimental values of q (not shown here) suggest the applicability of this model to represent the equilibrium adsorption of RhB dye onto the CGW/PPy composite. By comparison between Langmuir and Redlich–Peterson models, when β is near to 1.0 we can expect K_{RP}/a_R ratio similar to the adsorption

Table 1 Parameters of Langmuir and Freundlich models and percentage of deviation

q_{max}	K_L	R^2	% D
Langmuir model			
50.59	0.00333	0.9723	9.3
K_F	n	R^2	% D
Freundlich model			
1.397	2.0	0.9402	13.5
K_{RP}	a_R, β	R^2	% D
Redlich–Peterson model			
1.185	1.31×10^{-3}, 1.645	0.9791	6.0

monolayer capacity from the Langmuir equation. It can be observed from Table 1 that K_{RP}/a_R (4.01×10^3) was very different to q_{max}, which is the consequence of β value at 1.645. On the other hand, comparing β with $1/n$ from the Freundlich equation we can see that they are also very different ($1/n = 0.497$). Thus, we can say that adsorption mechanism can be described by a mixture of interactions on homogeneous and heterogeneous surface.

The maximum adsorption capacity of the CGW/PPy observed for the Langmuir model, was higher than the reported in literature with other adsorbents for the same dye; for example sodium alginate/hydroxyethyl cellulose/humic acid (SA/HEC/HA) membranes (18.8 mg/g) [45], expanded perlite (0.43 mg/g) [46], wall-nut shells (2.29 mg/g) [47]; and similar to activated carbon (42.90 mg/g) [48], sodium montmorillonite (42.2 mg/g) [49], and black tea leaves (53.2 mg/g) [50]; and lower than modified *Volvariella volvacea* (68.49 mg/g) [51], *Casuarina equisetifolia* needles (82.34 mg/g) [52], *Aleurites moluccana* seeds (117 mg/g) [53], and BPH activated carbon (263.85 mg/g) [54].

Conclusion

The composite of CGW/PPy was synthesized through chemical polymerization of pyrrole monomer and characterized. SEM analysis showed that PPy coating CGW consisted of spherical nanoparticles with sizes in the range of 100–250 nm. Due to the presence of PPy in the composite, lower thermal stability of composite with respect to an uncoated CGW was observed. However, decomposition rate of CGW/PPy composite was slower than the corresponding uncoated CGW. While testing the CGW/PPy composite in the RhB dye removal from aqueous solution, it was observed that adsorption is favored at basic pH due to the PZC of 3.2 of the composite and the negative form of RhB speciation under this pH condition. The Redlich–Peterson Langmuir model was the best model to describe the adsorption process with a maximum adsorption capacity of 50.59 mg/g.

Acknowledgements This work was supported by SEP-PRODEP (Mexico) through Program "Red de Investigación y Desarrollo de Nanomateriales Híbridos para Aplicaciones Ambientales Avanzadas".

Compliance with ethical standards

Conflict of interest The authors have declared no conflict of interest.

References

1. Noorhosseini A, Allahyari MS, Damalas CA, Moghaddam SS (2017) Public environmental awareness of water pollution from urban growth: the case of Zarjub and Goharrud rivers in Rasht, Iran. Sci Total Environ 599–600:2019–2025
2. WWAP (United Nations World Water Assessment Programme), The United Nations World Water Development Report (2017) Wastewater: the untapped resource. UNESCO, Paris
3. Drumond Chequer FM, Rodrigues de Oliveira GA, Anastácio Ferraz ER, Carvalho Cardoso J, Boldrin Zanoni MV, Palma de Oliveira D (2013) Textile Dyes: Dyeing Process and Environmental Impact. In: Gunay M (ed) Eco-Friendly Textile Dyeing and Finishing. InTech, Rijeka, pp 151–176
4. Purkait MK, Maiti A, DasGupta S, De S (2007) Removal of congo red using activated carbon and its regeneration. J Hazard Mater 145:287–295
5. Garg VK, Gupta R, Yadav AB, Kumar R (2003) Dye removal from aqueous solution by adsorption on treated sawdust. Bioresour Technol 89:121–124
6. Li Y, Chen W (2011) Photocatalytic degradation of rhodamine B using nanocrystalline TiO_2–zeolite surface composite catalysts: effects of photocatalytic condition on degradation efficiency. Catal Sci Technol 1:802–809
7. Shen K, Gondal MA (2017) Removal of hazardous rhodamine dye from water by adsorption onto exhausted coffee ground. J Saudi Chem Soc 21:S120–S127
8. Bardajee GR, Azimi S, Sharifi MBAS (2016) Ultrasonically accelerated synthesis of silver nanocomposite hydrogel based on salep biopolymer: application in rhodamine dye adsorption. Iran Polym J 25:1047–1063
9. Hayeeye F, Sattar M, Chinpa W, Sirichote O (2017) Kinetics and thermodynamics of rhodamine B adsorption by gelatin/activated carbon composite beads. Colloid Surf A Physicochem Eng Aspects 513:259–266
10. Shen J, Wu Y, Zhang B, Li F (2015) Adsorption of rhodamine B dye by biomimetic mesoporous SiO_2 nanosheets. Clean Technol Environ Policy 17:2289–2298
11. Baek MH, Ijagbemi CO, Se-Jin O, Kim DS (2010) Removal of malachite green from aqueous solution using degreased coffee bean. J Hazard Mater 176:820–828
12. Hirata M, Kawasaki N, Nakamura T, Matsumoto K, Kabayama M, Tamura T, Tanada S (2002) Adsorption of dyes onto carbonaceous materials produced from coffee grounds by microwave treatment. J Colloid Interface Sci 254:17–22
13. Safarik I, Horska K, Svobodova B, Safarikova M (2012) Magnetically modified spent coffee grounds for dyes removal. Eur Food Res Technol 234:345–350
14. Nabid MR, Sedghi R, Sharifi R, Oskooie HA, Heravi MM (2013) Removal of toxic nitrate ions from drinking water using conducting polymer/MWCNTs nanocomposites. Iran Polym J 22:85–92
15. Banimahd-Keivani M, Zare K, Aghaie H, Ansari R (2009) Removal of methylene blue dye by application of polyaniline nanocomposite from aqueous solutions. J Phys Theory Chem 6:50–56
16. Ansari R, Mosayebzadeh Z (2010) Removal of basic dye methylene blue from aqueous solutions using sawdust and sawdust coated with polypyrrole. J Iran Chem Soc 20107:339–350
17. Ovando-Medina VM, Díaz-Flores PE, Martínez-Gutiérrez H, Moreno-Ruiz LA, Antonio-Carmona ID, Hernández-Ordoñez M (2014) Composite of cellulosic agricultural waste coated with semi-conducting polypyrrole as potential dye remover. Polym Compos 35:186–193
18. Ovando-Medina VM, Vizcaíno-Mercado J, González-Ortega O, Rodríguez de la Garza JA, Martínez-Gutiérrez H (2015) Synthesis of α-cellulose/polypyrrole composite for the removal of reactive red dye from aqueous solution: kinetics and equilibrium modeling. Polym Compos 36:312–321

19. Lavecchia R, Medici F, Patterer MS, Zuorro A (2016) Lead removal from water by adsorption on spent coffee grounds. Chem Eng Trans 47:295–300
20. Mussatto SI, Ballesteros LF, Martins S, Teixeira JA (2011) Extraction of antioxidant phenolic compounds from spent coffee grounds. Sep Purif Technol 83:173–179
21. Johnston JH, Moraes J, Borrmann T (2005) Conducting polymers on paper fibres. Synth Met 153:65–68
22. Pujol D, Liu C, Gominho J, Olivella JA, Fiol N, Villaescusa I, Pereira H (2013) The chemical composition of exhausted coffee waste. Ind Crops Prod 50:423–429
23. Morán JI, Alvarez VA, Cyras VP, Vázquez A (2008) Extraction of cellulose and preparation of nanocellulose from sisal fibers. Cellulose 15:149–159
24. Li X, Tabil LG, Panigrahi S (2007) Chemical treatments of natural fiber for use in natural fiber-reinforced composites: a review. J Polym Environ 15:25–33
25. Johnston JH, Kelly FM, Moraes J, Borrmann T, Flynn D (2006) Conducting polymer composites with cellulose and protein fibres. Curr Appl Phys 6:587–590
26. Müller D, Rambo CR, Recouvreux DOS, Porto LM, Barra GMO (2011) Chemical in situ polymerization of polypyrrole on bacterial cellulose nanofibers. Synth Met 161:106–111
27. Wondraczek H, Kotiaho A, Fardim P, Heinze T (2011) Photoactive polysaccharides. Carbohydr Polym 83:1048–1061
28. Arjomandi J, Holze R (2013) A spectroelectrochemical study of conducting pyrrole-*N*-methylpyrrole copolymers in nonaqueous solution. J Solid State Electrochem 17:1881–1889
29. Ovando-Medina VM, Peralta RD, Mendizábal E, Martínez-Gutiérrez H, Lara-Ceniceros TE, Ledezma-Rodríguez R (2011) Synthesis of polypyrrole nanoparticles by oil-in-water microemulsion polymerization with narrow size distribution. Colloid Polym Sci 289:759–765
30. Omastová M, Trchová M, Kovárová J, Stejskal J (2003) Synthesis and structural study of polypyrroles prepared in the presence of surfactants. Synth Met 138:447–455
31. Ballesteros LF, Teixeira JA, Mussatto SI (2014) Chemical, functional, and structural properties of spent coffee grounds and coffee silverskin. Food Bioprocess Technol 7:3493–3503
32. Jakab E, Mészáros E, Omastová M (2007) Thermal decomposition of polypyrroles. J Therm Anal Calorim 88:515–521
33. Qi L, Tang X, Wang Z, Peng X (2017) Pore characterization of different types of coal from coal and gas outburst disaster sites using low temperature nitrogen adsorption approach. Int J Mining Sci Technol 27:371–377
34. Thommes M, Kaneko K, Neimark AV, Olivier JP, Rodriguez-Reinoso F, Rouquerol J, Sing KS (2015) Physisorption of gases, with special reference to the evaluation of surface area and pore size distribution (IUPAC Technical Report). Pure Appl Chem 87:1051–1069
35. Sing KSW, Williams RT (2004) Physisorption hysteresis loops and the characterization of nanoporous materials. Adsorpt Sci Technol 22:773–782
36. Franca AS, Oliveira LS, Ferreira ME (2009) Kinetics and equilibrium studies of methylene blue adsorption by spent coffee grounds. Desalination 249:267–272
37. Nyström G, Mihranyan A, Razaq A, Lindström T, Nyholm L, Strømme M (2010) A nanocellulose polypyrrole composite based on microfibrillated cellulose from wood. J Phys Chem B 114:4178–4182
38. González-Iñiguez JC, Ovando-Medina VM, Jasso-Gastinel CF, González DA, Puig JE, Mendizábal E (2014) Synthesis of polypyrrole nanoparticles by batch and semicontinuous heterophase polymerizations. Colloid Polym Sci 292:1269–1275
39. Salleh MAM, Mahmoud DK, Karim WAW, Idris A (2011) Cationic and anionic dye adsorption by agricultural solid wastes: a comprehensive review. Desalination 280:1–13
40. Thompson G, Swain J, Kay M, Forster CF (2001) The treatment of pulp and paper mill effluent: a review. Bioresour Technol 77:275–286
41. Giles CH, MacEwan TH, Nakhwa SN, Smith D (1960) Studies in adsorption. Part XI. A system of classification of solution adsorption isotherms, and its use in diagnosis of adsorption mechanisms and in measurement of specific surface areas of solids. J Chem Soc (Resumed) 0:3973–3993
42. Langmuir I (1918) The adsorption of gases on plane surfaces of glass, mica and platinum. J Am Chem Soc 40:1361–1403
43. Gerente C, Lee VKC, Cloirec PL, McKay G (2007) Application of chitosan for the removal of metals from wastewaters by adsorption—mechanisms and models review. Crit Rev Environ Sci Technol 37:41–127
44. Belhachemi M, Addoun F (2011) Comparative adsorption isotherms and modeling of methylene blue onto activated carbons. Appl Water Sci 1:111–117
45. Shenvi SS, Isloor AM, Shilton SJ, Al Ahmed A (2015) Humic acid based biopolymeric membrane for effective removal of methylene blue and rhodamine B. Eng Ind Chem Res 54:4965–4975
46. Damiyine B, Guenbour A, Boussen R (2017) Adsorption of rhodamine B dye onto expanded perlite from aqueous solution: kinetics, equilibrium and thermodynamics. J Mater Environ Sci 8:345–355
47. Shah J, Jan MR, Haq A, Khan Y (2013) Removal of rhodamine B from aqueous solutions and wastewater by walnut shells: kinetics, equilibrium and thermodynamics studies. Front Chem Sci Eng 7:428–436
48. Paulraj A, Elizabeth AT (2016) Removal of rhodamine B and congo red from aqueous solutions by adsorption onto activated carbons. Chem Sci Trans 5:87–96
49. Selvam PP, Preethi S, Basakaralingam P, Thinakaran N, Sivasamy A, Sivanesan S (2008) Removal of rhodamine B from aqueous solution by adsorption onto sodium montmorillonite. J Hazard Mater 155:39–44
50. Hossain MA, Alam MS (2012) Adsorption kinetics of rhodamine-B on used black tea leaves. Iran J Environ Health Sci Eng 9:2–15
51. Li Q, Tang X, Sun Y, Wang Y, Long Y, Jiang J, Xu H (2015) Removal of rhodamine B from wastewater by modified Volvariella volvacea: batch and column study. RSC Adv 5:25337–25347
52. Kooh MRR, Dahri MK, Lim LB (2016) The removal of rhodamine B dye from aqueous solution using Casuarina equisetifolia needles as adsorbent. Cogent Environ Sci. https://doi.org/10.1080/23311843.2016.1140553
53. Postai DL, Demarchi CA, Zanatta F, Melo DCC, Rodrigues CA (2016) Adsorption of rhodamine B and methylene blue dyes using waste of seeds of *Aleurites Moluccana*, a low cost adsorbent. Alexandr Eng J 55:1713–1723
54. Gad HMH, El-Sayed AA (2009) Activated carbon from agricultural by-products for the removal of rhodamine B from aqueous solution. J Hazard Mater 168:1070–1081